American Mineralogist, Volume 62, pages 1216–1224, 1977

Structural variation in the ferrobustamite solid solution

TAKAMITSU YAMANAKA, RYOICHI SADANAGA AND YOSHIO TAKÉUCHI

Mineralogical Institute, Faculty of Science
University of Tokyo, Hongo, Tokyo, Japan

Abstract

Ferrobustamite, $Wo_{82}Fs_{18}$, from the Ofuku mine, Yamaguchi Prefecture, Japan, is close to the Fe-poor end of the ferrobustamite solid solution. Its crystal data are: space group $A\bar{1}$, a = 7.862, b = 7.253, c = 13.967 A, α = 89°44′ β = 95°28′, γ = 103°29′, and $12[Ca_{0.82}Fe_{0.15}Mn_{0.03}SiO_3]$ in the unit cell. Our refinement of its structure reveals that it possesses pseudo-mirrors which are more nearly true mirror planes than those in the $Wo_{50}Fs_{50}$ structure, and the small size of one cation site, $M3$, in the structure induces the concentration of the Fe(Mn) content into it, thus giving the solid solution the Fe-poor limit of $Wo_{83.3}Fs_{16.7}$. The Mössbauer spectra of the specimen showed that, after a heat treatment at 1,140°C, the degree of concentration of Fe at $M3$ decreases, suggesting that the site occupancies of Fe atoms vary with the temperature of formation and the cooling process of the crystal.

Introduction

Bowen *et al.* (1933) presented a phase diagram of the system CaO–FeO–SiO_2 showing an extensive solid solution at temperatures above 1,000°C, and called it the "wollastonite solid solution." Tilley (1937) first described a mineral with a composition of 77 mole percent $CaSiO_3$ and 23 percent $FeSiO_3$ ($Wo_{77}Fs_{23}$) from Scawt Hill, County, Antrim, and named it "iron-wollastonite." He further reported another iron-wollastonite from contact skarns at Skye, Scotland (Tilley, 1948).

A reexamination by Rutstein (1971) of the $CaSiO_3$–$CaFeSi_2O_6$ system showed that there are two different phases in this system, and these are compositionally separated from each other by a gap extending from $Wo_{88}Fs_{12}$ to $Wo_{78}Fs_{22}$. Rutstein and White (1971) analyzed infrared spectra of these samples, and suggested that those rich in iron have a structure analogous to that of bustamite.

The crystal structures of two pyroxenoids, a synthetic phase, $Ca_{0.5}Fe_{0.5}SiO_3$ ($Wo_{50}Fs_{50}$), and a natural phase, $Ca_{0.79}Fe_{0.19}Mn_{0.02}SiO_3$ ($Wo_{79}Fs_{21}$), both refined by Rapoport and Burnham (1973), are similar to each other and to that of bustamite. This species was therefore named ferrobustamite by these authors, who pointed out that the Fe-poor end-member of this phase region is expected on structural grounds to lie at $Wo_{5/6}Fs_{1/6}$.

From chemical analyses of natural samples, Shimazaki and Yamanaka (1973) discovered a miscibility gap between wollastonite and ferrobustamite, and suggested that ferrobustamite with an Fe content larger than that of $Ca_{5/6}Fe_{1/6}SiO_3$ ($Wo_{83.3}Fs_{16.7}$) will be stable at the low temperatures appropriate for skarn formation, probably 300–600°C. Matsueda (1973, 1974) also reconfirmed that ferrobustamite is distinct from wollastonite in optical and chemical properties and cell dimensions, and considered paragenetic relations between ferrobustamite and wollastonite. Compositional limits of wollastonite, bustamite, and ferrobustamite were also discussed by Mason (1975).

Since the structure refinement of the natural phase, $Wo_{79}Fs_{21}$, reported by Rapoport and Burnham (1973), was hindered by the twinned crystal used for the structure determination, we consider it necessary to reexamine the structure with a well-specified crystal. Also the structure of ferrobustamite in the Fe-poor limit was of particular importance for clarifying structure variations of the solid solution. We have therefore undertaken a structural investigation of $Ca_{0.82}Fe_{0.15}Mn_{0.03}SiO_3$ and compared our results with the data previously obtained from other members of the series.

Refinement of the ferrobustamite structure

The crystal used in the present investigation was found in the Ofuku mine, Yamaguchi Prefecture,

Table 1. Chemical analyses of $Wo_{82}Fs_{18}$

	Weight% (1)	Weight% (2)		Mole% (3)
SiO_2	49.85	49.8	$CaSiO_3$	82.2
TiO_2	tr.	—	$FeSiO_3$	14.9
Al_2O_3	0.56	0.0	$MnSiO_3$	2.6
Fe_2O_3	0.33	—	$MgSiO_3$	0.3
FeO	8.64	9.0	Total	100.0
MnO	1.58	1.6		
MgO	0.21	0.1		
CaO	38.50	38.9		
Na_2O	0.02	—		
K_2O	0.02	—		
$H_2O(+)$	0.05	—		
$H_2O(-)$	0.12	—		
Total	99.91	99.4		

(1) *Wet chemical analysis by H. HARAMURA.*

(2) *Electron probe analysis.*

(3) *These values were calculated using the data from the electron probe analyzer.*

Japan. The chemical composition determined by an electron microprobe analysis is approximately $Ca_{0.82}Fe_{0.15}Mn_{0.03}SiO_3$ ($Wo_{82}Fs_{18}$), which is very close to, but has a slightly smaller Ca content than $Ca_{5/6}Fe_{1/6}SiO_3$, the Fe-poor compositional limit of ferrobustamite suggested by Rapoport and Burnham (1973) and Shimazaki and Yamanaka (1973). The chemical composition of the specimen is listed in Table 1. The lattice parameters are a = 7.862, b = 7.253, c = 13.967 A, α = 89°44′, β = 95°28′, γ = 103°29′, and its space group is $A\bar{1}$.

Intensities of 3083 reflections up to 2θ = 70° were measured with an automatic four-circle diffractometer with Mo$K\alpha$ radiation and a graphite monochromator. Reflections with integrated intensities lower than three times the standard deviation were ignored. The $\omega - 2\theta$ scanning was carried out at 1° in 2θ per minute. The intensities were corrected for Lorentz and polarization effects and subjected to absorption correction using the computer program ACACA written by C. T. Prewitt. As an initial model for our structure refinement, we adopted the atomic parameters given by Peacor and Buerger (1962) for the bustamite structure, and made a plausible assumption on the distribution of Fe atoms.

A full-matrix least-squares refinement was carried out using the program LINUS (Coppens and Hamilton, 1970). During the first two cycles of refinement, the scale factor and the isotropic extinction parameter were varied. Three successive cycles shifted atomic parameters and isotropic temperature factors, resulting in R=8.8 percent (non-weighted residual factor). The next three cycles varied site occupancies at the metal sites and reduced R to 5.6 percent. The refinement of anisotropic temperature factors was achieved in three more cycles. The final R value was then 3.5 percent. Atomic coordinates and anisotropic temperature factors thus attained are presented in Tables 2 and 3 respectively. Interatomic distances are given in Table 4. Observed and calculated structure factors are presented in Table 5.[1] Atomic coordinates and interatomic distances of the bustamite structure analyzed by Peacor and Buerger (1962) and ferrobustamite ($Wo_{50}Fs_{50}$) by Rapoport and Burnham (1973) are also presented in Tables 2 and 4 for comparison.

Structural variations due to Ca–Fe substitution

We shall here compare the structure of $Wo_{82}Fs_{18}$ with those of $Wo_{50}Fs_{50}$ and bustamite, thereby discussing some crystal chemical characteristics of the ferrobustamite solid solution. As discussed by Peacor and Prewitt (1963) on the structure relationship between wollastonite and bustamite, the ferrobustamite structure is characterized by the gliding by $b/2$ of unit slabs of wollastonite structure cut parallel to (001) and $d_{(001)}/2$ thick. The Ca(1) and Ca(2) sites in wollasonite nearly correspond respectively to the $M1$ and $M2$ sites in ferrobustamite. On the other hand, the Ca(3) site in wollastonite splits into two distinct sites in ferrobustamite, $M3$ and $M4$, at inversion centers. Among the four metal cation polyhedra in ferrobustamite, $M3$ is the smallest and $M4$ the largest (Table 4).

The four metal cation sites lie in a plane parallel to (102). Between two such cation layers silicate chains are located, each being a repetition of a unit of three tetrahedra, Si_3O_9, running parallel to the b axis.

Pseudomirror

The salient feature of the structure of ferrobustamites is that it is composed of a kind of substructure or a slab with cell dimensions (in the case of $Wo_{82}Fs_{18}$):

$$a_s \simeq t_{[\bar{4}10]}/4 = 7.645 \text{ A},$$

$$b_s = b = 7.253 \text{ A},$$

$$c_s \simeq c = 13.967 \text{ A},$$

[1] To receive a copy of Table 5, order document number AM-77-054 from the Business Office, Mineralogical Society of America, Suite 1000 lower level, 1909 K Street, N.W., Washington, D.C. 20006. Please remit $1.00 in advance for the microfiche.

and $\beta_s \simeq (100):(010) = 91°54'$,

where those with the suffix s are the constants of the substructure, the remainder the constants of the triclinic true cell, and $t_{[\bar{4}10]}$ indicates the unit lattice vector in the zone $[\bar{4}10]$. The symmetry of this substructure is pseudo-monoclinic (space group $A2/m$) with pseudo-mirror planes parallel to $(\bar{1}40)$ of the

Table 2. Atomic coordinates of ferrobustamite and bustamite

Atom	Ferrobustamite $Wo_{82}Fs_{18}$	Ferrobustamite $Wo_{50}Fs_{50}$ (1)	Bustamite (2)
M(1) 2*			
Occupancy	Ca:0.972(6) Fe:0.028(6)	Ca:0.23(1) Fe:0.77(1)	Ca Mn:1.000
x	0.2006(2)	0.2067(2)	0.2018
y	0.4175(2)	0.4266(2)	0.4284
z	0.3775(1)	0.3731(1)	0.3733
B	0.417(5)	0.93(3)	0.56
M(2) 2			
Occupancy	Ca:0.983(7) Fe:0.017(7)	Ca:0.78(1) Fe:0.22(1)	Ca:1.000 Mn
x	0.1988(1)	0.1989(2)	0.1988
y	0.9329(3)	0.9391(2)	0.9411
z	0.3757(1)	0.3759(1)	0.3785
B	0.536(7)	0.82(4)	0.69
M(3) 1			
Occupancy	Ca:0.035(6) Fe:0.965(6)	Ca:0.07 Fe:0.93	Ca Mn:1.000
x	1/2	1/2	1/2
y	1/4	1/4	1/4
z	1/4	1/4	1/4
B	0.505(8)	0.72(4)	0.56
M(4) 1			
Occupancy	Ca:0.986(6) Fe:0.014(6)	Ca:0.92(2) Fe:0.08(2)	Ca:1.000 Mn
x	1/2	1/2	1/2
y	3/4	3/4	3/4
z	1/4	1/4	1/4
B	0.536(7)	0.70(5)	0.73
Si(1) 2			
Occupancy	1.000	1.000	1.000
x	0.1888(1)	0.1751(3)	0.1768
y	0.3960(1)	0.3904(3)	0.3881
z	0.6365(2)	0.6368(2)	0.6343
B	0.355(7)	0.65(3)	0.34
Si(2) 2			
Occupancy	1.000	1.000	1.000
x	0.1925(1)	0.1775(3)	0.1775
y	0.9570(3)	0.9426(3)	0.9434
z	0.6315(3)	0.6312(2)	0.6325
B	0.631(6)	0.71(4)	0.32
Si(3) 2			
Occupancy	1.000	1.000	1.000
x	0.3971(2)	0.3935(3)	0.3950
y	0.7263(2)	0.7179(3)	0.7170
z	0.5231(2)	0.5226(1)	0.5218
B	0.349(5)	0.62(3)	0.16

Atom	Ferrobustamite $Wo_{82}Fs_{18}$	Ferrobustamite $Wo_{50}Fs_{50}$	Bustamite
O(1) 2			
Occupancy	1.000	1.000	1.000
x	0.4292(2)	0.4304(8)	0.4316
y	0.2346(1)	0.2376(9)	0.2400
z	0.4026(2)	0.4011(4)	0.4027
B	0.724(7)	0.80(9)	1.10
O(2) 2			
Occupancy	1.000	1.000	1.000
x	0.4008	0.4021(7)	0.4036
y	0.7237	0.7096(8)	0.7178
z	0.4085	0.4068(4)	0.4069
B	0.579	1.18(11)	0.57
O(3) 2			
Occupancy	1.000	1.000	1.000
x	0.3177	0.3141(8)	0.3126
y	0.4808	0.4724(9)	0.4725
z	0.7315	0.7312(4)	0.7293
B	0.687	1.18(10)	0.48
O(4) 2			
Occupancy	1.000	1.000	1.000
x	0.3103	0.3032	0.3017
y	0.9280	0.9279	0.9303
z	0.7292	0.7303	0.7315
B	0.900	1.00	0.48
O(5) 2			
Occupancy	1.000	1.000	1.000
x	0.0150	0.0276	0.0261
y	0.6213	0.6155	0.6167
z	0.3556	0.3510	0.3549
B	0.870	1.56	0.64
O(6) 2			
Occupancy	1.000	1.000	1.000
x	0.0129	0.0295	0.0280
y	0.1339	0.1638	0.1627
z	0.3738	0.3744	0.3717
B	1.043	1.76	0.66
O(7) 2			
Occupancy	1.000	1.000	1.000
x	0.2637	0.2540	0.2574
y	0.5183	0.5108	0.5047
z	0.5434	0.5424	0.5393
B	0.772	1.05	0.57
O(8) 2			
Occupancy	1.000	1.000	1.000
x	0.2787	0.2740	0.2728
y	0.8838	0.8800	0.8739
z	0.5400	0.5388	0.5411
B	0.823	1.01	0.29
O(9) 2			
Occupancy	1.000	1.000	1.000
x	0.2238	0.1866	0.1852
y	0.1860	0.1703	0.1676
z	0.6188	0.6176	0.6147
B	1.107	2.15	1.34

(1) From Rapoport and Burnham (1973).

(2) From Peacor and Buerger (1962).

* *This number indicates a multiplicity in the atomic site.*

The numbers in parentheses indicate standard deviations in the least significant figure.

Isotropic temperature factors represented by B were calculated from aniso temperature factors.

Table 3. Anisotropic temperature factors of $Wo_{82}Fs_{18}$

	β_{11}	β_{22}	β_{33}	β_{12}	β_{13}	β_{23}
M(1)	0.0021	0.0025	0.0006	0.0004	0.0001	0.0000
M(2)	0.0023	0.0027	0.0007	0.0004	0.0001	0.0000
M(3)	0.0022	0.0025	0.0007	0.0004	0.0001	0.0000
M(4)	0.0023	0.0027	0.0007	0.0004	0.0001	0.0000
Si(1)	0.0015	0.0018	0.0005	0.0003	0.0001	0.0000
Si(2)	0.0018	0.0021	0.0005	0.0003	0.0001	0.0000
Si(3)	0.0015	0.0018	0.0005	0.0003	0.0001	0.0000
O(1)	0.0031	0.0036	0.0009	0.0005	0.0002	0.0000
O(2)	0.0025	0.0029	0.0007	0.0004	0.0001	0.0000
O(3)	0.0030	0.0035	0.0009	0.0005	0.0002	0.0000
O(4)	0.0039	0.0045	0.0012	0.0007	0.0002	0.0000
O(5)	0.0038	0.0044	0.0011	0.0006	0.0002	0.0000
O(6)	0.0045	0.0052	0.0013	0.0008	0.0002	0.0000
O(7)	0.0033	0.0039	0.0010	0.0006	0.0002	0.0000
O(8)	0.0036	0.0042	0.0011	0.0006	0.0002	0.0000
O(9)	0.0048	0.0056	0.0014	0.0008	0.0003	0.0001

The expression used for the anisotropic temperature factors was $\exp -(\beta_{11}h^2 + \beta_{22}k^2 + \beta_{33}l^2 + 2\beta_{12}hk + 2\beta_{13}hl + 2\beta_{23}kl)$.

triclinic cell, just as in the wollastonite structure (Ito, 1950; Peacor and Prewitt, 1963).

Though members of the ferrobustamite solid solution are isostructural with bustamite (Peacor and Buerger, 1962), the mode of their simulating monoclinic symmetry varies with composition. The projections along the *b* axis of $Wo_{82}Fs_{18}$ and $Wo_{50}Fs_{50}$ in Figure 1 show that the pseudo-mirror perpendicular to *b* is closer to a true mirror in the former than in the latter; atoms related by these pseudo-mirror planes are more nearly superimposed in the former than in the latter. This tendency is in harmony with the fact that the local pseudo-mirrors in wollastonite are even closer to true local mirror symmetry (Ito *et al.*, 1969). The displacements between the true atomic positions and the positions due to the pseudo-symmetry in $Wo_{82}Fs_{18}$ and $Wo_{50}Fs_{50}$ are expressed by distances between pseudosymmetrically related atom pairs in Table 6. Atom displacements in wollastonite are also presented in Table 6 for comparison.

Table 4. Interatomic distances

	Ferrobustamite $Wo_{82}Fs_{18}$	Ferrobustamite $Wo_{50}Fs_{50}$(1)	Bustamite(2)
M(1)-O(1)	2.469(2)	2.432(6)	2.487
O(2)	2.418(2)	2.218(6)	2.294
O(4)	2.313(1)	2.164(6)	2.163
O(5)	2.308(2)	2.149(6)	2.135
O(6)	2.233(2)	2.031(7)	2.048
O(7)	2.403(2)	2.375(5)	2.337
mean	2.357	2.228	2.244
M(2)-O(1)	2.498(2)	2.418(6)	2.445
O(2)	2.452(2)	2.531(6)	2.519
O(3)	2.292(3)	2.245(6)	2.299
O(5)	2.383(3)	2.365(6)	2.390
O(6)	2.291(3)	2.292(7)	2.293
O(8)	2.368(2)	2.330(5)	2.358
O(9)	3.240(2)	2.889(7)	2.894
mean(I)*	2.381	2.364	2.384
mean(II)**	2.503	2.439	2.457
M(3)-O(1)	2.249(2)	2.192(5)	2.215
O(3)	2.136(2)	2.138(6)	2.161
O(4)	2.188(2)	2.195(6)	2.231
mean	2.191	2.175	2.202
M(4)-O(2)	2.409(2)	2.348(5)	2.345
O(3)	2.442(2)	2.375(6)	2.402
O(4)	2.462(3)	2.420(6)	2.429
O(9)	2.658(3)	2.827(7)	2.888
mean(I)*	2.438	2.381	2.392
mean(II)**	2.493	2.493	2.516
Si(1)-O(3)	1.621(2)	1.613(7)	1.630
O(5)	1.592(3)	1.574(6)	1.581
O(7)	1.648(2)	1.643(5)	1.647
O(9)	1.633(3)	1.613(6)	1.616
mean	1.624	1.611	1.619
Si(2)-O(4)	1.616(2)	1.617(6)	1.625
O(6)	1.590(2)	1.583(7)	1.585
O(8)	1.648(2)	1.641(6)	1.644
O(9)	1.633(3)	1.618(6)	1.613
mean	1.622	1.615	1.618
Si(3)-O(1)	1.606(2)	1.601(6)	1.599
O(2)	1.604(2)	1.603(6)	1.596
O(7)	1.664(2)	1.640(5)	1.665
O(8)	1.663(2)	1.665(6)	1.664
mean	1.634	1.627	1.631

(1) *From Rapoport and Burnham (1973).*

(2) *Recalculated from the data published by Peacor and Buerger (1962).*

* *Mean value including M-O(9).*

** *Mean value excluding M-O(9).*

The numbers in parentheses indicate standard deviations in the least significant figures.

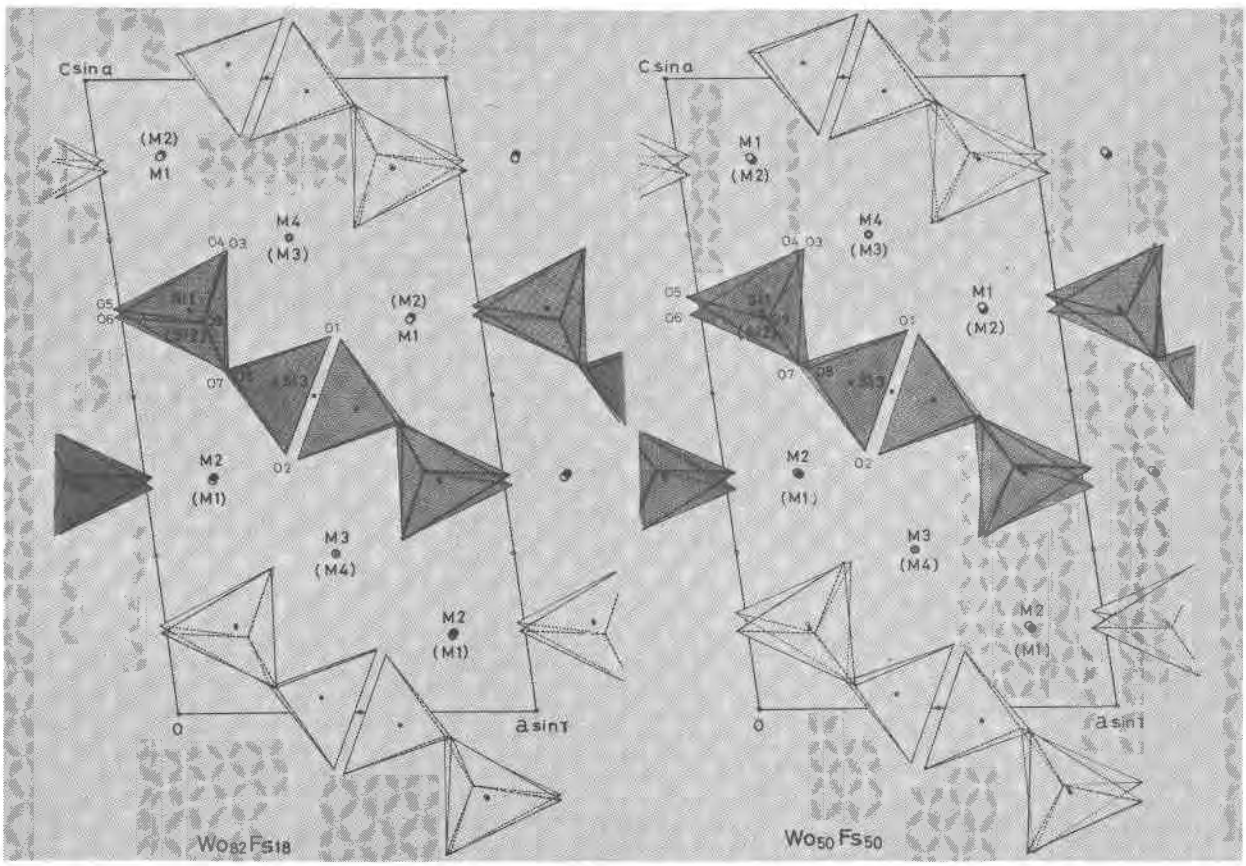

Fig. 1. The structures of $Wo_{82}Fs_{18}$ and $Wo_{50}Fs_{50}$, each projected along the *b* axis. The pseudo-mirror perpendicular to the *b* axis is more distinct in $Wo_{82}Fs_{18}$ than is $Wo_{50}Fs_{50}$. O(1), O(2), O(9), and Si(3) are placed on a pseudo-mirror plane. All the other atoms are located in pairs separated by about *b*/2. Pairs of shaded triplets of tetrahedra are shifted by *b*/2 from those of unshaded ones.

Table 6. Deviations of atom pairs from true mirror symmetry

	Wollastonite	Ferrobustamite	
	$Wo_{100}Fs_0$	$Wo_{82}Fs_{18}$	$Wo_{50}Fs_{50}$
M(1)-M(2) Ca(1)-Ca(2)	0.0047 Å	0.0032 Å	0.0159 Å
M(3)-M(4) Ca(3)-Ca(3)'	0.0004	0	0
Si(1)-Si(2)	0.0008	0.0109	0.0082
Si(3)-Si(3)'	0.0008	0.0033	0.0061
O(1)-O(1)'	0.0004	0.0036	0.0083
O(2)-O(2)'	0.0015	0.0017	0.0212
O(3)-O(4)	0.0019	0.0066	0.0080
O(5)-O(6)	0.0023	0.0256	0.0368
O(7)-O(8)	0.0085	0.0182	0.0190
O(9)-O(9)'	0.0007	0.0086	0.0030
mean	0.0022	0.0082	0.0127

For each pair of atoms, which are related to each other by a pseudo mirror plane, the deviation from true mirror is expressed by the distance between one atom of the pair and an atom which would be related to the other if the pseudosymmetry were true mirror.

Compositional limit and site occupancies

As referred to in the foregoing section, the ferrobustamite structure is characterized by the gliding by *b*/2 of unit slabs. This gliding causes the Ca(3) site in the wollastonite structure to split into two crystallographically distinct sites in the ferrobustamite structure, *M*3 and *M*4. The size differences between the four metal cation coordination polyhedra determine the site occupancies of Ca and Fe. The smallest *M*3 polyhedra are certainly better able to accommodate the smaller Fe atom. As reported by Rapoport and Burnham (1973), based on their structural study of ferrobustamites, this situation accounts for the Ca-rich compositional limit, $Ca_{5/6}Fe_{1/6}SiO_3$, of the ferrobustamite solid solution. Takéuchi *et al.* (1976) have observed that the same conclusion can be drawn from the features of cation ordering observed in the serandite–pectolite series. In the ferrobustamite, whose composition almost corresponds to the Ca-rich limit, Fe is indeed preferentially located at *M*3 (Table 2).

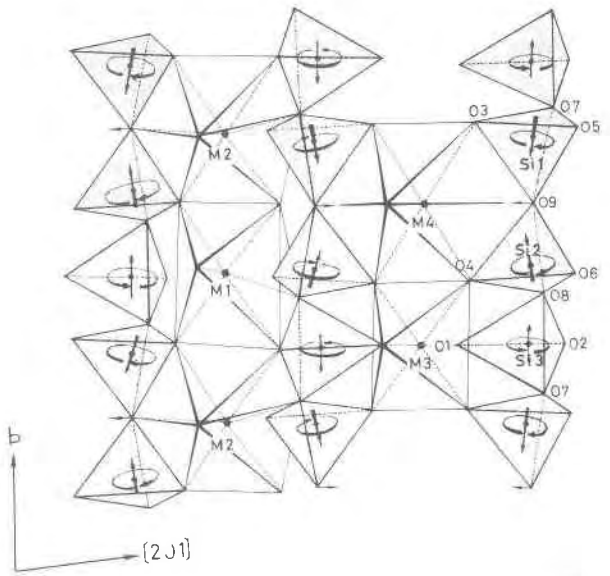

Fig. 2. Projection of the structure of ferrobustamite on to (102), showing the movement of silicate chains due to change in composition from $Wo_{50}Fs_{50}$ to $Wo_{82}Fs_{18}$. Arrows at oxygen atoms and in the silicate tetrahedra indicate respectively the direction of movement of the atoms and tetrahedra. An extreme expansion of the $M1$ site due to the substitution of Ca for Fe in the site induces the rotation of silicate tetrahedra as indicated, reducing the bond angle Si(1)–O(9)–Si(2). The rotation axes at Si(1) and Si(2) are tilted from the plane of projection roughly by 15° for $Wo_{50}Fs_{50}$ and 20° for $Wo_{82}Fs_{18}$; the movements of tetrahedra are in fact expressed by rotations about these axes combined with the movement of the axes as suggested by the difference in tilting angle.

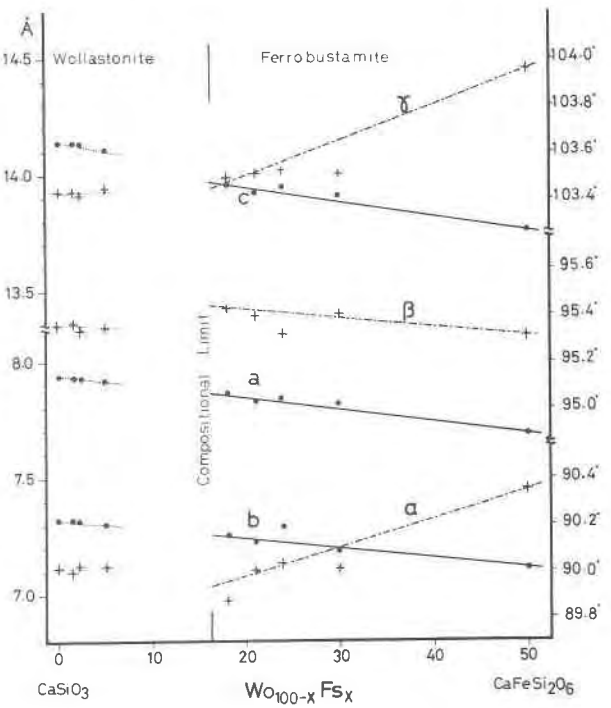

Fig. 3. Variation of cell parameters in the ferrobustamite solid solution. Those of $Wo_{50}Fs_{50}$ and $Wo_{79}Fs_{21}$ are from Rapoport and Burnham (1973), and those of $Wo_{70}Fs_{30}$ from Matsueda (1973). Others are obtained in the present study by least-squares refinement using powder diffraction data. The space group of ferrobustamite is described in terms of the A-centered cell.

In bustamite with the ideal composition $CaMnSi_2O_6$, Ca and Mn atoms are ordered; one Ca atom and one Mn atom are located at the Ca(2) site and the Mn(2) site which correspond respectively to $M4$ and $M3$ in ferrobustamite, and two Ca atoms and two Mn atoms at Ca(1) and Mn(1) corresponding respectively to $M2$ and $M1$. A slight excess of Ca from the ideal composition in the bustamite specimen studied by Peacor and Buerger (1962) replaces Mn at the Mn(1) ($M1$) site. On the other hand, Mn(2) ($M3$) accommodates very little Ca (Ohashi and Finger, 1975), which is in harmony with the fact that Mn(2) ($M3$) has the smallest coordination polyhedron. Based on the results of these studies, the variation of cation site occupancies in the bustamite solid solution is also given in Figure 4 for comparison.

Si_3O_9 chain and cell parameters

Owing to Ca–Fe substitution in the ferrobustamite solid solution, the configuration of silicate chains varies considerably, as shown in Table 7. With increasing amounts of the larger cation, Ca, in ferrobustamite structure, the tetrahedra rotate as shown in Figure 2. Since thermal expansion of cation polyhedra is in general geometrically similar to the expansion due to cation substitution, thermal expansion of

Table 7. Si–Si and O–O distances and Si–O–Si angles

		Ferrobust.		
	Woll.	$Wo_{82}Fs_{18}$	$Wo_{50}Fs_{50}$	Bust.
O(3)-O(4)	3.473 Å	3.258 Å	3.259 Å	3.297 Å
O(5)-O(6)	3.616	3.540	3.234	3.263
O(7)-O(8)	4.682	4.632	4.526	4.545
Si(1)-Si(2)	3.165	3.192	3.190	3.184
Si(2)-Si(3)	3.125	3.070	3.043	3.077
Si(1)-Si(3)	3.116	3.092	3.060	3.065
Si(1)-O(7)-Si(3)	139.24°	137.96°	137.50°	135.42°
Si(2)-O(8)-Si(3)	140.19	135.97	134.01	137.04
Si(1)-O(9)-Si(2)	149.14	155.56	162.49	160.74

These data of Woll., $Wo_{50}Fs_{50}$, and Bustamite are recalculated from the data published by Peacor and Prewitt (1963), Rapoport and Burnham (1973) and Peacor and Buerger (1962).

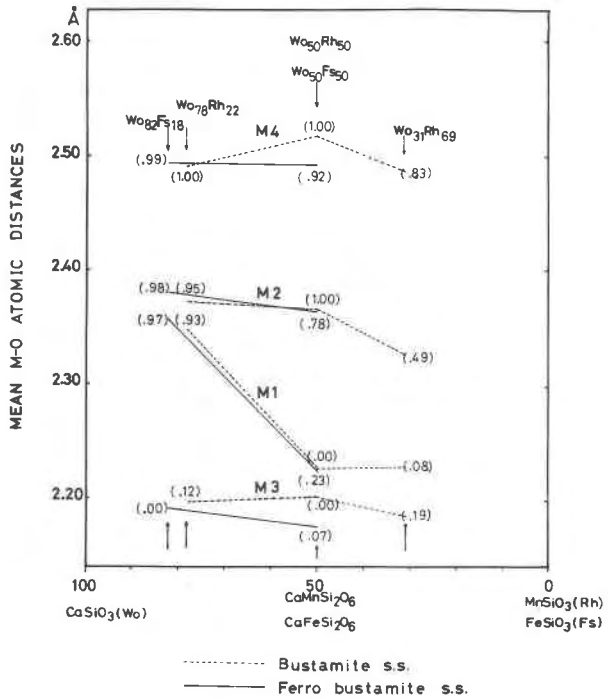

Fig. 4. Variation of M–O interatomic distances of polyhedra in the ferrobustamite and bustamite solid solution. The numbers in parentheses indicate the site occupancies of Ca atoms in four sites in the two series. Mean interatomic distance of the $M(2)$ site excludes the $M(2)$–O(9) distance. The data of bustamite solid solution are obtained from Ohashi and Finger (1975) and Peacor and Buerger (1962). Those of $Wo_{50}Fs_{50}$ in ferrobustamite solid solution are from Rapoport and Burnham (1973).

the cation octahedra in ferrobustamite would be expected to impose a similar rotation effect upon silicate tetrahedra. It has in fact been shown by Takéuchi (1971) that a gliding by $b/2$ of a silicate chain, which is in general required in transformations in the wollastonite-group minerals, can be effected not by actual translation by $b/2$ of the chain but by simple rotations (or twistings) of its constituent tetrahedra.

The structure variation due to Ca–Fe substitution in the ferrobustamite solid solution is reflected in its cell parameters, as shown in Figure 3. As evident from the figure, the cell dimensions a, b, and c, change linearly in the same way, indicating that the larger the Ca content the larger the dimension. This figure also shows that, when extrapolated, the trend of each of the parameters is not linearly connected to the corresponding one of the wollastonite solid solution. This is consistent with the results of Rutstein (1971), indicating that the changes of some d-values show a sudden break at around $Wo_{88}Fs_{12}$.

Thermal variation of cation ordering

The variation in site occupancies in $Wo_{82}Fs_{18}$ induced by heat treatment was studied with the aid of Mössbauer spectra. It was confirmed by EPMA analyses and X-ray precession photographs that the sample, after being heated at 1,140°C for 96 hours in an evacuated silica tube, remains unaltered both chemically and structurally, although site occupancies differ in detail. At temperatures above

Table 8. Parameters of Mössbauer spectra

Sample (Treatment)	Site	I.S. (mm/sec)	Q.S. (mm/sec)	Half Width (mm/sec)	Peak Intensity (%)
$Wo_{88}Fs_{12}$ (No heat treatment)	M3	1.34(3)	3.01(6)	0.31(2)	93.5
	M1	1.33(3)	2.26(5)	0.29(2)	6.5
$Wo_{88}Fs_{12}$ (Heating at 1140°C for 96 hours in the evacuated tube)	M3	1.37(3)	3.07(6)	0.31(2)	66.8
	M1	1.32(3)	2.11(5)	0.32(2)	25.3
	M2	1.32(3)	1.48(5)	0.28(2)	7.9

The spectra obtained at a constant Doppler velocity calibrated by those in metallic iron were analyzed with the aid of a computer program which performed the fitting of experimental data to the Lorentzian function by a least mean square method.

I.S. represents the isomer shifts which were measured with reference to that of 310 stainless steel. Q.S. represents the quadrupole splittings.

Standard deviations in parentheses represent uncertainty in the least significant figures.

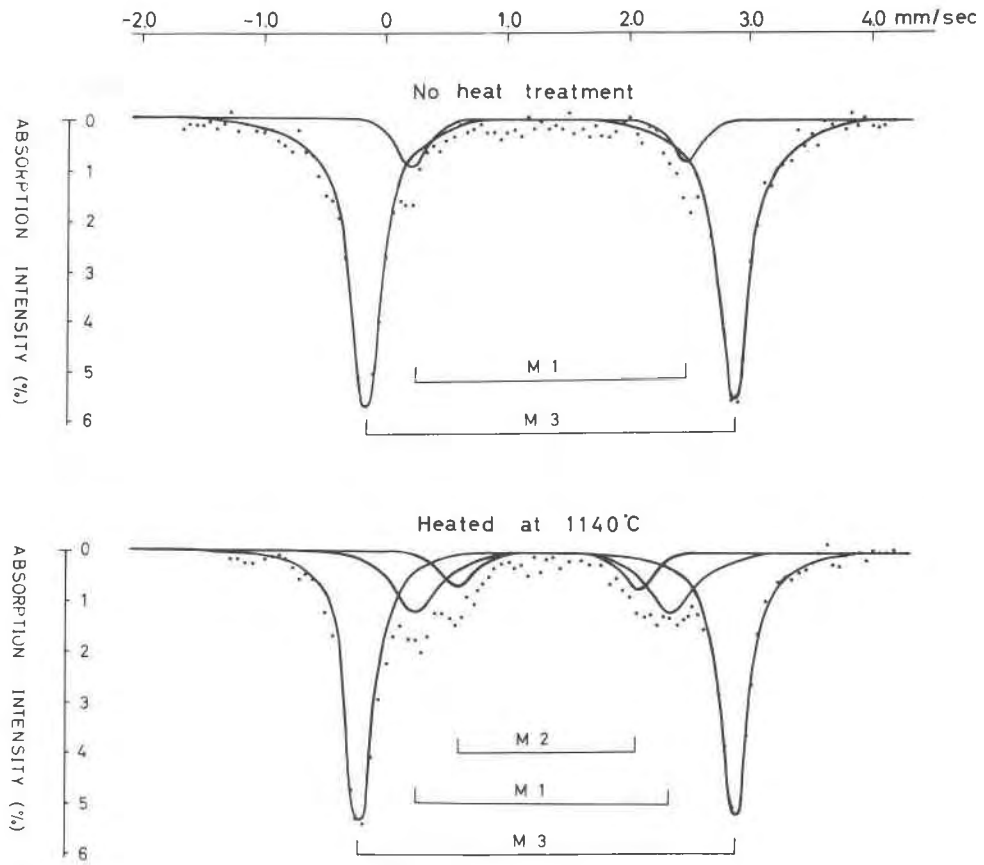

Fig. 5. Mössbauer spectra of ^{57}Fe in $Wo_{82}Fs_{18}$ before and after heat treatment at 1140°C. Thermal effect on the site occupancies is proved by the change of peak intensity ratios of Fe atoms in the $M1$, $M2$, and $M3$ sites. The isomer shift (I.S.) expressed relatively to the spectrum of 310 stainless steel, and the Doppler velocity is calibrated with the spectrum of metallic iron.

1,160°C the sample is transformed into one having both the wollastonite and parawollastonite structures, which will shortly be reported elsewhere.

The Mössbauer spectra of ^{57}Fe of the sample before and after the heat treatment were obtained at room temperature by the experimental technique described in previous reports (Yamanaka, 1973; Yamanaka and Kato, 1976). The spectra thus obtained were analyzed with the aid of a computer program which performs least-squares fit of the observed data to a Lorentzian curve. The variable parameters were peak position, full width at the half-maximum intensity, peak intensity, and background level of the off-resonance count. The isomer shift, quadrupole splitting, line width at the half-maximum intensity, and peak intensity are shown in Table 8.

The result indicates that before heating as much as 93.5 percent of the Fe content in $Wo_{82}Fs_{18}$ is concentrated at one site, which probably corresponds to $M3$ and the remaining 6.5 percent occupies another site, probably $M1$, based on comparison with the site occupancies determined by X-ray means and given in Table 2. However, as seen in the variation in peak intensities in Figure 5, after heat treatment the concentration of Fe at $M3$ decreases to 66.8 percent, whereas those at $M1$ and $M2$ increase.

The quadrupole splitting at $M3$ is a little larger after the heat treatment than before, while that at $M1$ shows a reverse tendency. Since the quadrupole splitting depends on the gradient of the electric field at an Fe nucleus that is induced by the valence electrons of the Fe atom and the surrounding anions (Ingalls, 1962, 1964), the above facts indicate that the variations in site occupancies at these sites have caused some change in coordination polyhedra formed by oxygen atoms about certain Fe atoms in the site. On the other hand, the identical value of isomer shift for each of these sites before and after the heat treatment reveals that the Fe atoms share the same ionic character.

From the thermal change in site occupancies established above, it is suggested that the less orderly cation distribution in the $Wo_{50}Fs_{50}$ structure studies by Rapoport and Burnham (1973) was due to the high temperature of 1,000°C at which their sample was synthesized.

The results of the present study suggest that in the process of decompositional transformation from ferrobustamite to wollastonite, Fe, preferentially located in the $M3$ site at low temperatures, is redistributed into $M1$ and $M2$ giving a more disordered ferrobustamite structure that then transforms to wollastonite.

Acknowledgments

The authors are indebted to Dr. H. Shimazaki, Geological Institute, University of Tokyo, and Dr. Y. Ohashi, Geology Department, University of Pennsylvania, for their discussions and furnishing information at various stages of this study, and also to Mr. H. Haramura for chemical analysis.

References

Bowen, N. L., J. F. Schairer and E. Posnjak (1933) The system CaO–FeO–SiO_2. *Am. J. Sci., 26,* 193–284.

Coppens, P. and Hamilton, W. C. (1970) Anisotropic extinction corrections in the Zachariasen approximation. *Acta Crystallogr., A26,* 71–83.

Ingalls, R. (1962) Radiational calculation of the Sternheimer factors for the ferrous ion. *Phys. Rev., 128,* 1155–1158.

——— (1964) Electric field gradient tensor in ferrous compounds. *Phys. Rev., 133,* A787–795.

Ito, T. (1950) *X-ray Studies on Polymorphism.* Maruzen, Tokyo.

———, R. Sadanaga, Y. Takéuchi and M. Tokonami (1969) The existence of partial mirror in wollastonite. *Proc. Japan Acad., 45,* 913–918.

Mason, B. (1975) Compositional limits of wollastonite and bustamite. *Am. Mineral., 60,* 209–212.

Matsueda, H. (1973) Iron wollastonite from the Sampo mine showing properties distinct from those of wollastonite. *Mineral. J. (Japan), 7,* 180–201.

——— (1974) Immiscibility gap in the system $CaSiO_3$–$CaFeSi_2O_6$ at low temperatures. *Mineral. J. (Japan), 7,* 327–343.

Ohashi, Y. and L. W. Finger (1975) Cation ordering and crystal structures of Ca-rich and Ca-poor bustamite (abstr.). *Geol. Soc. Am. Abstracts with Programs, 7,* 216.

Peacor, D. and M. J. Buerger (1962) Determination and refinement of the crystal structure of bustamite, $CaMnSi_2O_6$. *Z. Kristallogr., 117,* 335–343.

——— and C. T. Prewitt (1963) Comparison of the crystal structures of wollastonite and bustamite. *Am. Mineral., 48,* 588–596.

Rapoport, P. and C. W. Burnham (1973) Ferrobustamite: The crystal structure of two Ca,Fe bustamite-type pyroxenoids. *Z. Kristallogr., 138,* 419–438.

Rutstein, M. S. (1971) Reexamination of the wollastonite–hedenbergite ($CaSiO_3$–$CaFeSi_2O_6$) equilibria. *Am. Mineral., 56,* 2040–2052.

——— and W. B. White (1971) Vibrational spectra of high-calcium pyroxenes and pyroxenoids. *Am. Mineral., 56,* 877–887.

Shimazaki, H. and T. Yamanaka (1973) Iron wollastonite from skarns and its stability relation in the $CaSiO_3$–$CaFeSiO_6$ join. *Geochem. J.* (Japan), *7,* 67–79.

Takéuchi, Y. (1971) Polymorphic or polytypic changes in biotites, pyroxenes and wollastonite. *J. Mineral. Soc. Japan, 10,* S87–102.

———, Y. Kudoh and T. Yamanaka (1976) Crystal chemistry of the serandite–pectolite series and related minerals. *Am. Mineral., 61,* 229–237.

Tilly, C. E. (1937) Wollastonite solid solution from Scawt Hill, Co., Antrim. *Mineral. Mag., 24,* 569–572.

——— (1948) On iron–wollastonites in contact skarns: an example from Skye. *Am. Mineral. 33,* 736–738.

Yamanaka, T. (1973) Variation of site occupancy of the spinel solid solutions of Fe_3O_4–Mn_3O_4 and Fe_3O_4–Fe_2TiO_4. *J. Crystallogr. Soc. Japan, 17,* 181–190.

——— and A. Kato (1976) Mössbauer effect study of ^{57}Fe and ^{119}Sn in stannite, stannoidite, and mawsonite. *Am. Mineral., 61,* 260–265.

Manuscript received, September 9, 1976; accepted for publication, June 28, 1977.